Direct determination of the $f(\alpha)$ singularity spectrum and its application to fully developed turbulence

Ashvin B. Chhabra, Charles Meneveau,* Roderick V. Jensen, and K. R. Sreenivasan
Mason Laboratory, Yale University, P.O. Box 2159, New Haven, Connecticut 06520
(Received 22 June 1989)

This paper focuses on a method proposed for determining $f(\alpha)$ (the singularity spectrum of a multifractal) directly from experimental data, without first calculating the "generalized dimensions" D_q and applying the usual Legendre transforms. We describe the method, which is based on theorems by Shannon, Eggelston, and Billingsley, and apply it to one-dimensional cuts of the dissipation field of fully developed turbulence in laboratory and atmospheric flows. The accuracy of this method can be understood in terms of computation of conventional thermodynamic quantities in microcanonical and canonical ensembles. Comparisons with other direct and indirect methods of computing $f(\alpha)$ are made.

I. INTRODUCTION

It is now widely accepted that physical systems that exhibit chaotic behavior are generic in Nature. Since these systems lose information exponentially fast it is possible to follow and predict their motion in any detail only for short time scales. To describe their long-term dynamical behavior, one must resort to suitable statistical descriptions. One such description is the multifractal formalism.[1-4]

The multifractal formalism relies on the fact that the highly nonuniform probability distributions arising from the nonuniformity of the system often possess rich scaling properties including that of self-similarity. The study of the long-term dynamical behavior of the physical system can then be attempted by the characterization of the fractal properties of a measure that can be associated with the nonuniform distribution. Some examples are the spatial distribution of dissipative regions in a turbulent flow,[5-7] the invariant probability distribution on a strange attractor,[4] the distribution of voltage drops across a random resistor network,[8] and the distribution of growth probabilities on the external surface of a diffusion-limited aggregate.[9] For general reviews on the field see Refs. 10 and 11.

The multifractal formalism describes the statistical properties of these singular measures in terms of their singularity spectrum,[3,4] or their generalized dimensions.[2] In particular, if we cover the support of the measure with boxes of size l and define $P_i(l)$ to be the probability (integrated measure) in the ith box, then we can define an exponent (singularity strength) α_i by

$$P_i(l) \sim l^{\alpha_i} . \tag{1}$$

If we count the number of boxes $N(\alpha)$ where the probability P_i has singularity strength between α and $\alpha+d\alpha$, then $f(\alpha)$ can be loosely defined[4] as the fractal dimension of the set of boxes with singularity strength α by

$$N(\alpha) \sim l^{-f(\alpha)} . \tag{2}$$

This formalism leads to the description of a multifractal measure in terms of interwoven sets of Hausdorff dimension $f(\alpha)$ possessing singularity strength α.[3,4] On the other hand, the generalized dimensions D_q, which correspond to scaling exponents for the qth moments of the measure, provide an alternative description of the singular measure.[1,2,12] Once again, if we cover the support of the measure with boxes of size l and define $P_i(l)$ to be the probability in the ith box, then one can define a series of exponents parametrized by q according to

$$\sum_i P_i^q(l) \sim l^{(q-1)D_q} . \tag{3}$$

For mathematical reasons one is often interested in the limit of the box size going to zero leading to the conventional definition

$$D_q = \frac{1}{(q-1)} \lim_{l \to 0} \frac{\ln \sum_i P_i^q(l)}{\ln(l)} . \tag{4}$$

In the literature, the generalized dimensions were introduced earlier than the singularity spectrum and have been easier to compute than the latter, which accounts for their wide usage. The generalized dimensions are exponents that characterize the nonuniformity of the measure; positive q's accentuate the denser regions and negative q's accentuate the rarer ones. In addition, for certain special values of q one can intuitively recognize D_q as the dimension of a special set, which supports a particular part of the measure. For example, $D_{q=0}$ is the dimension of the support of the measure, and $D_{q=1}$ is the dimension of the measure-theoretic support of the measure (also known as the information dimension). More generally, the geometric meaning of the other D_q's can be understood as the dimensions of the set, which when used to intersect the measure creates a divergence of moments of order q or higher.[12] In contrast to the complicated geometrical interpretation of the D_q's, the $f(\alpha)$ singulari-

ty spectrum[3,4] provides a precise and intuitive description of the multifractal measure in terms of interwoven sets, with differing singularity strengths α, whose Hausdorff dimension is $f(\alpha)$.

When $f(\alpha)$ and D_q are smooth functions of α and q, $f(\alpha)$ is simply related to $\tau(q)=(q-1)D_q$ by a Legendre transformation.[3,4] This relationship is a natural consequence of a deep connection of the multifractal formalism with that of equilibrium statistical mechanics.[13–17] In particular, $\tau(q)$ and q are conjugate thermodynamic variables to $f(\alpha)$ and α. Given one of the smooth functions, e.g., the D_q curve, one can easily transform it to the $f(\alpha)$ curve. In fact, since the D_q's have, in the past, been easier to evaluate for measures arising from real or computer experiments, the $f(\alpha)$ curves have usually been determined by the Legendre transform of the $\tau(q)$ curve. For these reasons, one is led to believe that knowing one of them is as good as knowing the other. That is correct in theory but not in practice. There are two reasons: Firstly, the log-log plots involved in the measurement of D_q's, rather than showing perfect linear behavior, tend to be modulated by oscillations (due to lacunarity) and show scatter (usually because of insufficient data). The existence of these problems is well known and they are commonly encountered in the analysis of data from laboratory experiments; for example, in fluid turbulence and in structures such as the Hénon attractor. The analysis of such data for its scaling information involves finding an approximately linear region in a log-log plot of the qth moment of the measure with respect to the box size. Each such exponent has its own error bars, dependent among other things on the value of q. The D_q's corresponding to large negative q's may have large error bars, as they correspond to rarely occurring events of low intensity, and therefore depend on the number of points in the sample and the relation of the chosen box size to the underlying dynamics. Legendre transforming such a curve, which we know only at a finite number of points with variable precision, makes the error bar estimation in the new formalism a hazardous task.

The situation gets more complicated when discontinuities exist in the D_q curve. This corresponds to a phase transition in equilibrium statistical mechanics, and it is now well known that such transitions occur frequently in nonhyperbolic systems (and in higher-dimensional hyperbolic systems). The logistic map $X_{(n+1)}=AX_{(n)}(1-X_{(n)})$ at $A=4$ is one such example.[18,19] In such cases, the smoothing procedure can cause several problems (as discussed in some detail by Grassberger, Badii, and Politi.[19]) In addition, the analytic Legendre transform relation breaks down in such cases, making it more difficult to extract the $f(\alpha)$ from the D_q curve. Therefore one is motivated to find a way to directly determine $f(\alpha)$ from experimental data without resorting to the intermediate Legendre transform.

One might expect that Eqs. (1) and (2) provide us with a straightforward method of computing $f(\alpha)$ directly. For example, one could cover a given measure with boxes of size l, and compute the probability in each box. Equation (1) would then assign an exponent α_i to the ith box. Counting the number of boxes $N(\alpha)$ that possess a particular singularity strength α, and plotting that quantity against the box size l on a log-log plot would yield $-f(\alpha)$ as its slope. However, following such a procedure for finite data yields inaccurate answers due to poor convergence to asymptotic values. For example, Mandelbrot[12] has noted that for the binomial measure (two-scale Cantor measure) the entire $f(\alpha)$ curve visibly overshoots are true value even after using 10^{15} boxes (or intervals). Similar overshoots or undershoots are evident in other methods proposed to directly compute $f(\alpha)$ from data.[19–21] The reason for the overshoot are the scale-dependent prefactors in Eq. (2).[20,22] While such overshoots are not a problem if one first computes and then Legendre transforms the D_q curve, such a method has several other disadvantages as discussed earlier.

II. THEORY

We will discuss a new method to directly compute $f(\alpha)$ that was recently proposed in Ref. 23. The idea was to focus on the fact that $f(\alpha)$ is simply the dimension of the measure-theoretic support of a particular measure[25,12,17,23] (i.e., the complement of the set has zero Lebesgue measure). For a special class of measures that arise from multiplicative processes one can prescribe a recipe for computing $f(\alpha)$ as follows.

Cover the experimental measure with boxes of size l and compute the probability in each of these boxes $P_i(l)$. Then construct a one-parameter family of normalized measures $\mu(q)$ where the probabilities in the boxes of size l are

$$\mu_i(q,l)=\frac{[P_i(l)]^q}{\sum_j [P_j(l)]^q} . \tag{5}$$

As in the definition of the generalized dimensions, Eq. (4), the parameter q provides a microscope for exploring different regions of the singular measure. For $q>1$, $\mu(q)$ amplifies the more singular regions of the measure, while for $q<1$, it accentuates the less singular regions, and for $q=1$ the measure $\mu(1)$ replicates the original measure. Then the Hausdorff dimension of the measure-theoretic support of $\mu(q)$ is given by[23–26]

$$\begin{aligned} f(q) &= -\lim_{N\to\infty}\frac{1}{\ln N}\sum_{i=1}^{N}\mu_i(q,l)\ln\mu_i(q,l) \\ &= \lim_{l\to 0}\frac{\sum_i \mu_i(q,l)\ln\mu_i(q,l)}{\ln l} . \end{aligned} \tag{6}$$

In addition, the *average value* of the singularity strength $\alpha_i=\ln(P_i)/\ln l$ with respect to $\mu(q)$ can be computed by evaluating

$$\begin{aligned} \alpha(q) &= -\lim_{N\to\infty}\frac{1}{\ln N}\sum_{i=1}^{N}\mu_i(q,l)\ln P_i(l) \\ &= \lim_{l\to 0}\frac{\sum_i \mu_i(q,l)\ln P_i(l)}{\ln l} . \end{aligned} \tag{7}$$

Equations (6) and (7) provide a relationship between a

Hausdorff dimension f and an average singularity strength α as implicit functions of the parameter q. Moreover, it is easy to exploit the relationship of these definitions of $f(q)$ and $\alpha(q)$ to the definition of the generalized dimensions in Eq. (3) to show[4] that $f=q\alpha-\tau$ and $\alpha=d\tau/dq$, these being the Legendre transform relations already mentioned. Therefore Eqs. (6) and (7) provide an alternative definition of the singularity spectrum, which can be used to compute the $f(\alpha)$ curves directly from experimental data without the intermediate Legendre transform of the $\tau(q)$ curve.

In Ref. 23 this method was used to analyze a two-scale (binomial) Cantor measure. This measure is constructed by considering a unit interval and dividing it into two equal parts with unequal probabilities p_1 and p_2 on each part. This process is continued such that at each stage of refinement, each of the pieces of length l breaks up into two new pieces of length $l/2$ but unequal probabilities in the ratio p_1 and p_2 to the previous piece. It was shown that when box sizes were chosen of the form 2^{-n} ($n=1,2,3,\ldots$), thus optimally covering the pieces to reflect the multiplicative process giving rise to the measure, the log-log plots from Eqs. (6) and (7) were straight lines and the resultant $f(\alpha)$ curve was in exact agreement with the theoretical curve. However, if box sizes were chosen to some other base [e.g., $(1.1)^{-n}$], then the log-log plots from Eqs. (6) and (7) were straight lines modulated by oscillations through which least-squares fits were made, thus giving rise to error bars when calculating the $f(\alpha)$ curve. Despite these errors, the method reproduced most of the $f(\alpha)$ curve accurately, including the peak value which corresponds to the Hausdorff dimension of the support of the original measure D_0 and the Hausdorff dimension of the measure-theoretic support of the measure D_1 (at $f=\alpha$).

In this paper we will apply this method to determine the scaling properties of the dissipation field of fully developed turbulence. In addition, we will discuss the thermodynamic interpretation of this method and show that other methods of directly computing $f(\alpha)$ overshoot or undershoot the values of D_0 and D_1 due to finite-size corrections arising from logarithmic prefactors in Eq. (2).

III. APPLICATIONS TO FULLY DEVELOPED TURBULENCE

In turbulent flows, the transfer of kinetic energy from the large scales of motion to the smaller ones can be thought of as arising from a multiplicative cascade process. The manifestation of this flux of kinetic energy at the smallest scales is the rate of dissipation ε, which is defined as

$$\varepsilon=\frac{\nu}{2}\left[\frac{\partial u_i}{\partial x_j}+\frac{\partial u_j}{\partial x_i}\right]^2, \tag{8}$$

where u_i is the component of the turbulent velocity in direction x_i and ν is the kinematic viscosity. Expectations of a multiplicative cascading process lead us to believe that ε could have a multifractal distribution in physical, three-dimensional space. For general literature on this subject see Refs. 1 and 27–34.

Analnous to Eq. (1), one can now define a scaling exponent α in terms of the total dissipation $(E_l)_i$, which occurs in a box of size l at a position given by the index i according to

$$(E_l)_i=l^{\alpha_i}. \tag{9}$$

In Ref. 33 the $f(\alpha)$ curve of one-dimensional sections through the three-dimensional distribution was obtained using the moment exponents (generalized dimensions) D_q and then applying the Legendre transform. Here we wish to apply the method of obtaining $f(\alpha)$ directly from Eqs. (6) and (7) in order to illustrate the usefulness of the method and to show that the results are in good agreement with the previous measurements of Ref. 33. We consider two turbulent flows: a turbulent boundary layer of moderate Reynolds number ($R_\lambda\sim110$) and a high-Reynolds-number flow ($R_\lambda\sim1500$) in the atmospheric surface layer. (Note that R_λ is an internal Reynolds number based on the root-mean-square fluctuation velocity and the so-called Taylor microscale λ defined in Appendix A. R_λ is proportional to the square root of the usual Reynolds number based on the integral length scale.)

The data are obtained from measurements of time series of the streamwise velocity component $u_1(t)$ using hot-wire anemometry. As usual, Taylor's frozen-flow hy-

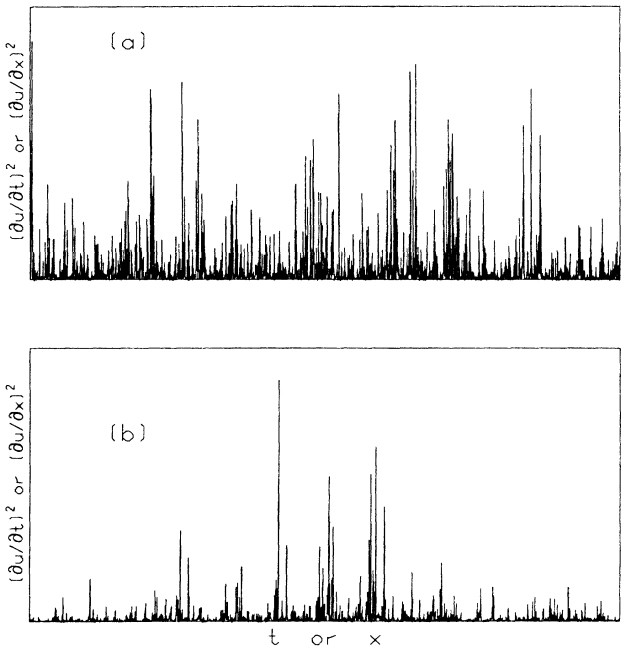

FIG. 1. Typical signals intepreted as representative of the dissipation rate ε on a one-dimensional cut through the instantaneous three-dimensional field of dissipation using Taylor's frozen-flow hypothesis. (a) From a flow in the laboratory boundary layer at a moderate Reynolds number $R_\lambda=110$ (see Appendix A). (b) From the atmospheric surface layer at high Reynolds number $R_\lambda>1500$ (see Appendix B).

pothesis is used to justify considering the time series obtained at a single point as a linear cut through the "frozen" turbulent velocity field in the streamwise direction. Furthermore, it is assumed that the gradient of only one velocity component in one direction is representative of the dissipation (which actually consists of nine terms). Therefore the dissipation is defined as

$$\varepsilon \sim (du_1/dt)^2 , \tag{10}$$

where the derivative was obtained by finite differences. The resulting data sets can be considered as one-dimensional cuts through a three-dimensional field. Details of the experimental conditions can be found in Appendixes A and B. Figure 1 shows typical signals of ε in the two flows considered. These distributions can be thought of as resulting from a multiplicative process, where the higher Reynolds number corresponds to more stages of the process.

In order to obtain $f(q)$ and $\alpha(q)$ we define a normalized measure μ_i in the ith box in terms of the dissipation field according to

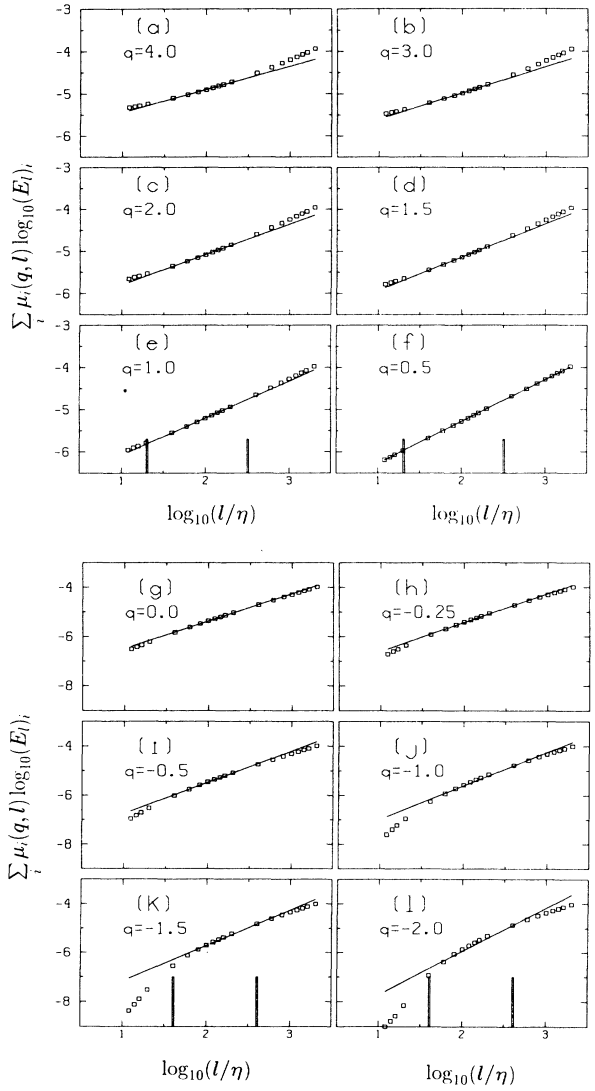

FIG. 2. (a)–(f) Plots of $\sum_i \mu_i(q,l)\log_{10}(E_l)_i$ vs $\log_{10}(l)$ for different positive q values for the laboratory boundary layer flow. The slopes of these graphs are $\alpha(q)$. The scaling range (indicated by vertical bars) is about 1.2 decades. (g)–(l) Plots of (the internal energy) $\sum_i \mu_i(q,l)\log_{10}(E_l)_i$ vs $\log_{10}(l)$ for different negative q values for the laboratory boundary layer flow. The slopes of these graphs are $\alpha(q)$. The scaling range (indicated by vertical bars) is about a decade.

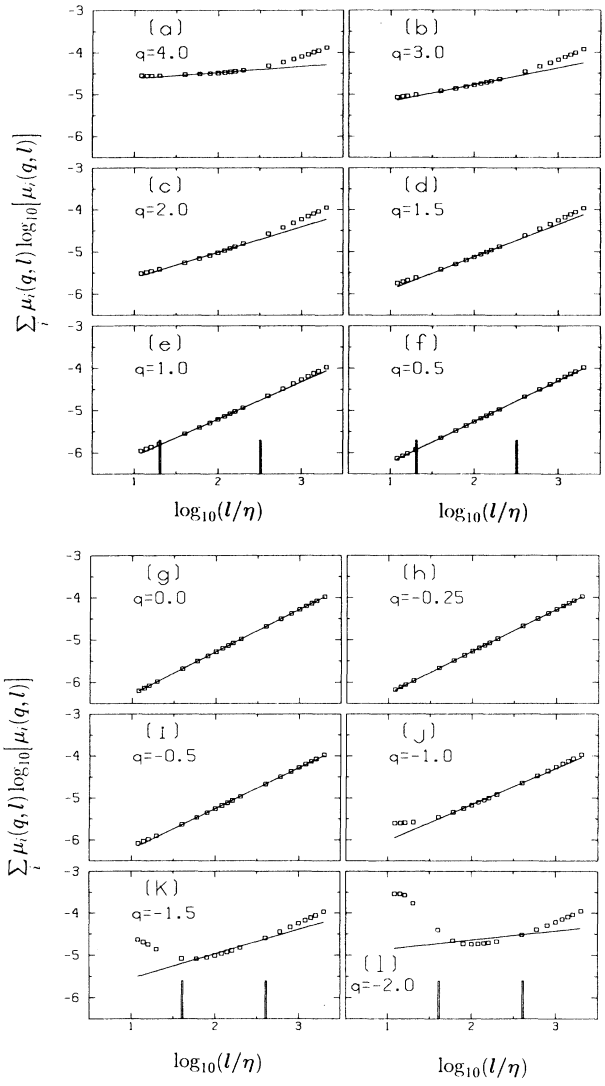

FIG. 3. (a)–(f) Plots of $\sum_i \mu_i(q,l)\log_{10}[\mu_i(q,l)]$ vs $\log_{10}(l)$ for positive values of q for the laboratory boundary-layer flow. The slopes of these graphs are $f(q)$. The scaling range (indicated by vertical bars) is identical to that in Fig. 2. (g)–(l) Plots of (the entropy) $\sum_i \mu_i(q,l)\log_{10}[\mu_i(q,l)]$ vs $\log_{10}(l)$ for negative values of q for the laboratory boundary-layer flow. The slopes of these graphs are $f(q)$. The scaling range (indicated by vertical bars) is identical to that in Fig. 2.

$$\mu_i(q,l)=(E_l)_i^q/\sum_j (E_l)_j^q \ , \tag{11}$$

where, again, the sum in the denominator is evaluated over all the boxes j of size l. According to Eqs. (6) and (7), plots of $\sum_i \mu_i(q,l)\log_{10}(E_l)_i$ versus $\log_{10}(l)$ will have slopes equal to $\alpha(q)$, whereas plots of $\sum_i \mu_i(q,l)\log_{10}[\mu_i(q,l)]$ versus $\log_{10}(l)$ will yield slopes equal to $f(q)$.

We first analyze the data from the laboratory boundary layer at a Reynolds number of about ($R_\lambda \sim 110$). Figures 2(a)–2(l) show the linear scaling obtained by computing $\sum_i \mu_i(q,l)\log_{10}(E_l)_i$ versus $\log_{10}(l)$. (In all the figures, the box size l will be normalized by the Kolmogorov scale η. Such a normalization only causes a translation of the abscissa and does not affect the exponents.) Similarly, Figs. 3(a)–3(l) show the scaling behavior of $\sum_i \mu_i(q,l)\log_{10}(\mu_i)$ versus $\log_{10}(l)$ for various values of q. The scaling range is a function of the Reynolds number and at this Reynolds number is not large. The linear scaling for positive q is shown as solid lines calculated by least-squares error fits in a range indicated by the vertical error bars, which for positive q is slightly more than one decade. One must take note of two aspects for negative q plots. These are discussed in Refs. 20 and 35 and Appendix A. Briefly, these correspond to regions of low dissipation and thus the results are more likely to be corrupted by noise in the data. In addition, there is another source of error in this region because of occasional nonturbulent portions of fluid. This has an effect of creating boxes with spuriously low values of dissipation in them, which are emphasized when the probability in each box is raised to a negative q value. These spurious contributions can degrade the true scaling of the data for $q < 1$.

In Fig. 4 we compare the $f(\alpha)$ curve generated by this method with those of previous results[5] generated by Legendre transforming the measured $\tau(q)$ curve. There is good agreement between the two curves. Since the latter curve is the Legendre transformation of an average of several $\tau(q)$ curves, accurate estimation of error bars is difficult. Nevertheless, it appears that it yields adequate results in the present instance.

We now analyze data corresponding to the dissipation field of the atmospheric surface layer. Figures 5(a)–5(l) show the linear scaling obtained by computing $\sum_i \mu_i(q,l)\log_{10}(E_l)_i$ versus $\log_{10}(l)$. Similarly, Figs. 6(a)–6(l) show the linear scaling obtained by computing

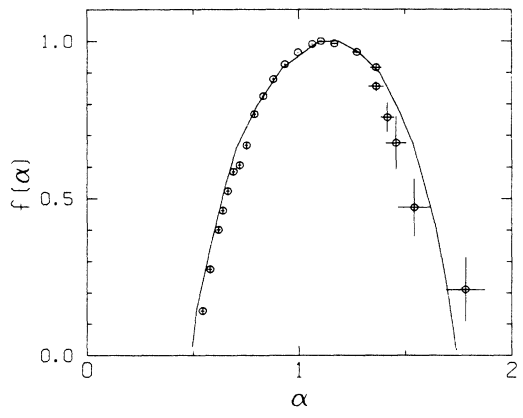

FIG. 4. Comparison of the $f(\alpha)$ curve of the dissipation field of one-dimensional sections of the flow in a laboratory boundary layer, using the (canonical) direct method discussed in Sec. II (circles) and from Legendre transforming several averaged $\tau(q)$ curves (solid lines). The agreement between the two curves is quite good.

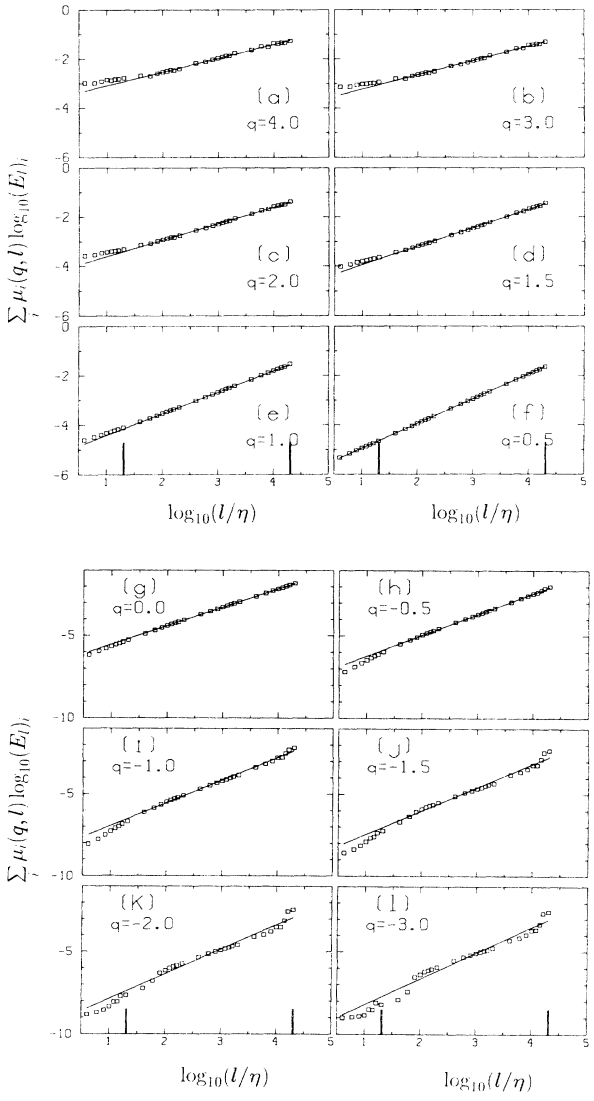

FIG. 5. (a)–(f) Plots of $\sum_i \mu_i(q,l)\log_{10}(E_l)_i$ vs $\log_{10}(l)$ for positive values of q for the atmospheric boundary-layer flow. The slopes of these graphs are $\alpha(q)$. The scaling range indicated by vertical bars is about three decades. Oscillations are visible for high values of $|q|$. (g)–(l) Plots of (the internal energy) $\sum_i \mu_i(q,l)\log_{10}(E_l)_i$ vs $\log_{10}(l)$ for negative values of q for the atmospheric boundary-layer flow. The slopes of these graphs are $\alpha(q)$. The scaling range indicated by vertical bars is the same as that in (a)–(f). Oscillations are visible for high values of $|q|$.

$\sum_i \mu_i(q,l)\log_{10}(\mu_i)$ versus $\log_{10}(l)$ for various different values of q. The high Reynolds number ($R_\lambda \sim 1500$) results in scaling over almost three decades. In Fig. 7 we show the $f(\alpha)$ curve computed for the atmospheric surface layer. We note that $D_0 = 1$, which tells us, once again, that there is no undershoot or overshoot of the entire curve. In addition, in Fig. 7 we compare the $f(\alpha)$ curve generated by this method with those of previous results[33] generated by Legendre transforming the $\tau(q)$ curve. Once again there is good agreement between the two curves.

Finally, we note that these $f(\alpha)$ curves give us the Hausdorff dimensions of the various iso-α sets of the dissipation field of turbulence. If the Reynolds number is sufficiently high, so that one is in the region of fully developed turbulence, then the various $f(\alpha)$ curves computed from data from various different experiments (i.e., an atmospheric surface layer, a laboratory boundary layer, the wake of a cylinder, and a turbulent flow behind a grid) are identical to within experimental accuracy.[33] In particular, the reader should compare Fig. 4 with Fig. 7.

Such results are consistent with the idea of a universal distribution of the small scales of turbulence, which does not depend on the details of the flow. The expectation of scale similarity at small scales arises from the fact that at high Reynold numbers viscosity effects are negligible. In the absence of this term, the Navier-Stokes equations become invariant under scale transformations. In addition, the randomizing effect of turbulence causes the small-scale structure to be largely independent of the large-scale structure, which may depend on the boundary conditions. These considerations are at the heart of the arguments leading to the classic $-\frac{5}{3}$ spectral exponent in Fourier space,[27] and have also been the motivating factor for the creation of various cascade models used to describe turbulence.[1,3,5,31,34]

In Sec. IV we compare this method (hereafter referred to as the canonical method) with other methods recently proposed to compute $f(\alpha)$ directly. We present an explanation of why these latter methods overshoot or undershoot the true curve and examine the circumstances under which these differences are significant.

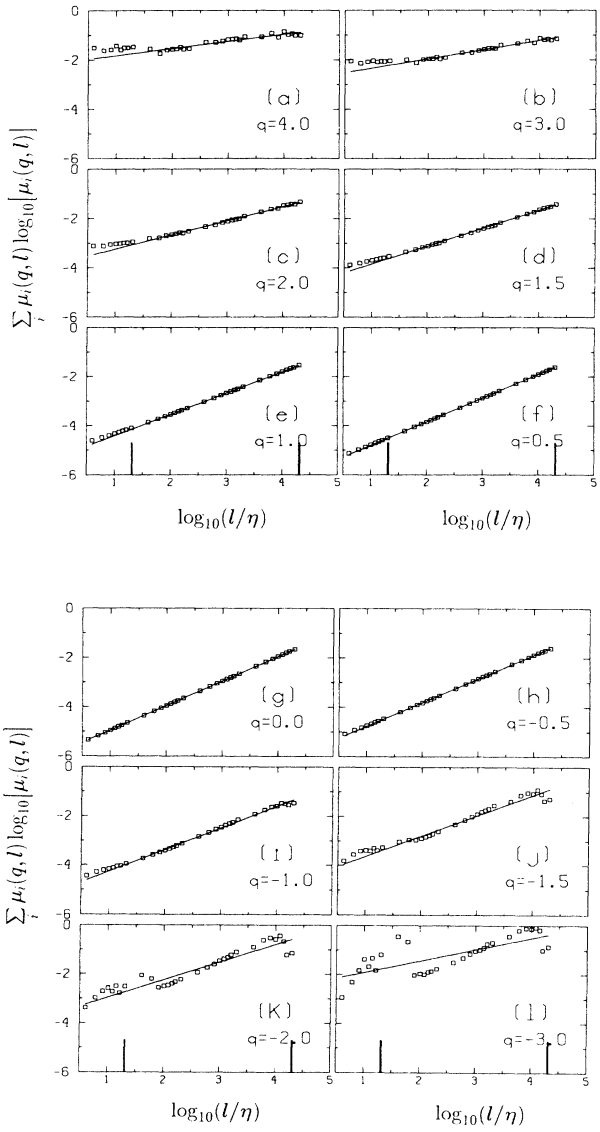

FIG. 6. (a)–(f) Plots of $\sum_i \mu_i(q,l)\log_{10}(\mu_i)$ vs $\log_{10}(l)$ for positive values of q for the laboratory boundary-layer flow. The slopes of these graphs are $f(q)$. The scaling range is identical to that in Fig. 5. (g)–(l) Plots of the entropy $\sum_i \mu_i(q,l)\log_{10}(\mu_i)$ vs $\log_{10}(l)$ for negative values of q for the laboratory boundary-layer flow. The slopes of these graphs are $f(q)$. The scaling range is identical to that in Fig. 5.

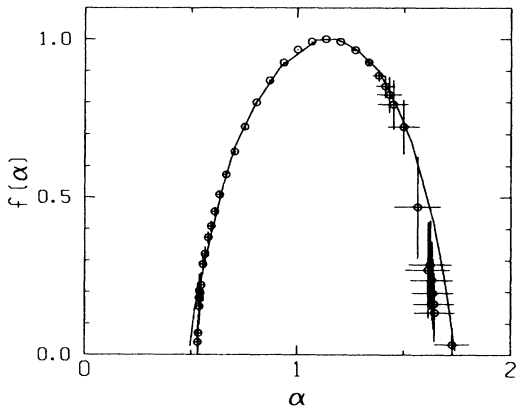

FIG. 7. Comparison of the $f(\alpha)$ curve of the dissipation field of one-dimensional sections of the flow in the atmosphere using the (canonical) direct method discussed in Sec. II (circles) and from Legendre transforming several averaged $\tau(q)$ curves (solid line). The agreement between the two curves is quite good.

IV. DIRECT DETERMINATION OF $f(\alpha)$ BY HISTOGRAMS

Recently, several other methods have been proposed to compute $f(\alpha)$ directly from multifractal measures. The starting point is the observation that one should be able to obtain α and $f(\alpha)$ directly from Eqs. (1) and (2). However, by naively taking the logarithms of these equations, one is usually left with adjustable constants due to the fact that one does not know the precise numerical prefactors to the power laws. In order to circumvent this difficulty, Arneodo, Grasseau, and Kostelich[36] assumed that these prefactors were constants independent of α or q, and determined them by numerical fits based on data from three different length scales (box sizes). Such a method presents difficulties when analyzing experimental or numerical data where cutoffs terminate the power laws at length scales that may not be known *a priori*, when there are oscillations around power laws, or when the preexponential terms depend on α. It is generally recognized that for the practical determination of scaling exponents it is usually better to consider several different length scales and obtain the exponents from regression plots. This idea was developed in Ref. 20 to obtain α and $f(\alpha)$ from the scaling properties of histograms.

However, both methods present problems as Eq. (2) is not exact at finite length scales because the normalization requirement of the total measure necessitates prefactors that depend on $\log_{10}(1/l)$ (and its powers). We first elaborate on this point, and summarize the method of obtaining $f(\alpha)$ directly by histograms[20] before applying it to the turbulent dissipation fields described previously. The purpose is both to illustrate its utility and shortcomings. Before doing so, however, the reader should notice that the problems of normalization discussed below are clearly absent in the method described in Sec. II.

Let us focus on how to evaluate the preexponential factors in Eq. (2). As recognized by van de Water and Schram,[22] the normalization of the total measure requires that

$$\sum_i P_i^q \Big|_{q=1} = \int C\rho(\alpha)(l)^{\alpha-f(\alpha)}d\alpha = 1 \ . \tag{12}$$

Expanding $f(\alpha)$ up to second order around α^* [minimizing $\alpha - f(\alpha)$] and evaluating the above integral by steepest descent gives

$$C\rho(\alpha^*)\left[\frac{2\pi}{\ln(1/l)|f''(\alpha^*)|}\right]^{1/2} l^{\alpha^*-f(\alpha^*)} = 1 \tag{13}$$

for any l. Since the power-law dependence of l is absorbed in $f(\alpha)$, the dependence of C on l cannot be a power law. This condition thus implies that

$$C = \rho(\alpha^*)^{-1}\left[\frac{2\pi}{|f''(\alpha^*)|}\right]^{1/2}\sqrt{\ln(1/l)} \ . \tag{14}$$

Therefore the leading correction to Eq. (2) is of the order $\sqrt{\ln(1/l)}$. Following Ref. 22, higher-order corrections in Eq. (2) can be taken into account by expanding $\rho(\alpha)$ to second order and $f(\alpha)$ to the fourth order. This leads to a normalization constant of the form

$$C = C_0(\alpha^*)\sqrt{\ln(1/l)}\left[1+\frac{C_1(\alpha^*)}{\ln(1/l)}\right], \tag{15}$$

where the coefficients C_0 and C_1 depend on the functions $\rho(\alpha)$, $f(\alpha)$, and their higher-order derivatives all evaluated at $\alpha^* = \alpha\ (q=1)$.[20,22]

This shows that the proportionality constant in Eq. (2) has to depend on powers of $\ln(1/l)$ and that Eq. (2) should be replaced by

$$N(\alpha)d\alpha \sim \sqrt{\ln(1/l)}\{1 + C_2(\alpha_{q=1})[\ln(1/l)]^{-1} + \cdots\}(l)^{-f(\alpha)}d\alpha \ . \tag{16}$$

Measuring the slope of the regression plots to determine $f(\alpha)$ corresponds to taking the derivative of the logarithm of Eq. (16) with respect to $\ln(1/l)$. After simple manipulations, one obtains

$$d\{\ln[N(\alpha)d\alpha]\}/d[\ln(l)] = -f(\alpha) - [2\ln(1/l)]^{-1} + C_2(\alpha_{q=1})[\ln(1/l)]^{-2} + \cdots, \tag{17}$$

which would correspond to the slope of log-log plots. This shows that these slopes would yield the correct $f(\alpha)$ only up to order $[\ln(1/l)]^{-1}$, this being the reason for the observation[12,19,20,23] that $f(\alpha)$ obtained along these lines overshoots considerably its asymptotic values, the error diminishing very slowly as $[\ln(1/l)]^{-1}$.

It was shown in Ref. 20 that one can thus correct for the first term (as was also done by Grassberger, Badii, and Politi[19]). Higher-order corrections cannot be determined accurately from experimental data.

For purposes of comparison, we now briefly summarize the method of scaling of histograms of Ref. 20. One defines a quantity X as the logarithm of the total measure $P_i(L)$ contained in each box

$$X_i(l) = \log_{10}[P_i(l)] \ , \tag{18}$$

which varies from box to box. For a given box size l, X will assume values that fluctuate between some limits, say, $X_{\min}(l)$ and $X_{\max}(l)$. It is easy to see that if one plots the values of $X_{\max}(l)$ as a function of $\log_{10}(l)$, the slope of the graph will correspond to $\alpha_{\min}$. Similarly, the slope of $X_{\min}$ versus $\log_{10}(l)$ corresponds to $\alpha_{\max}$. In order to obtain intermediate values of α, the interval $[X_{\min}(l), X_{\max}(l)]$ is discretized into pieces of equal length ΔX, and plots of these intermediate values of $X(l)$ versus $\log_{10}(l)$ will yield slopes of α that are intermediate between $\alpha_{\min}$ and $\alpha_{\max}$.

In order to obtain the exponent $f(\alpha)$ one constructs histograms of the different values of $X_i(l)$. Suppose that one counts $N_l(X)\Delta X$, which is the number of boxes of size l such that the variable X takes on a value in some interval ΔX around X. It was shown in Ref. 20 that in order to absorb the first-order correction in Eq. (14), one could divide $N(X)\Delta X$ by $\Delta X^{1/2}$. Therefore if one plots double logarithmic plots of $N(X)\Delta X^{1/2}$ versus l, the slope should be $f(\alpha)$ plus some error of order $\log_{10}(1/l)^{-2}$. Thus the error can be small if the available

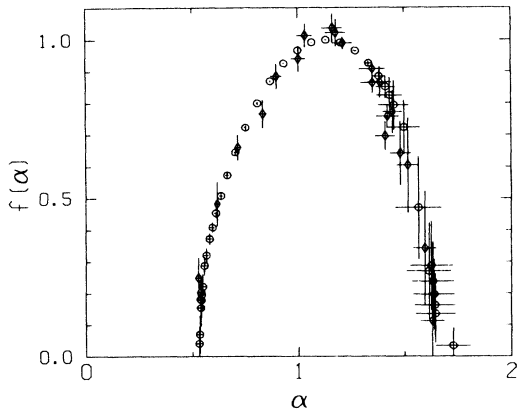

FIG. 8. Comparison of the $f(\alpha)$ curve using the method of scaling of histograms (diamonds) and the (canonical) method (circles) for the flow in an atmospheric surface layer. The good agreement is due to the large scaling range available at high Reynolds numbers. Terms in the order of $[\ln(1/l)]^{-2}$ that are neglected by the histogram method (Ref. 20) are negligible in this case.

scaling range is large, or substantial if the scaling range is small.

We now illustrate this method by applying it to the same turbulence data analyzed in Sec. III. In Fig. 8 we compare the $f(\alpha)$ curve obtained by the method of scaling of histograms with that of the canonical method for data from the high-Reynolds-number atmospheric flow. There is good agreement of the two curves as well as that obtained from previous results by Legendre transforming the $\tau(q)$ curves. This is because three decades of scaling makes the second-order correction term $[\log_{10}(1/l)]^{-2}$ negligible. However, for the laboratory flow case (Fig. 9)

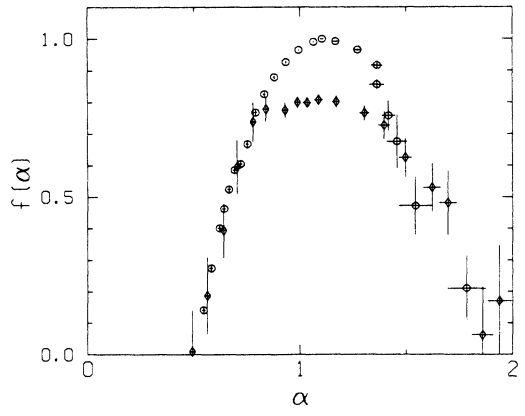

FIG. 9. Comparison of the $f(\alpha)$ curve using the methods of scaling the histograms (diamonds) and the (canonical) method (circles) for the boundary layer flow. The significant discrepancy is due to the small scaling range available at the moderate Reynolds numbers in the boundary layer. Terms in the order of $[\ln(1/l)]^{-2}$ become important and incorrectly bias the $f(\alpha)$ values obtained from the histogram method.

where only about one decade of scaling was available, the second-order correction term $[\log_{10}(1/l)]^{-2}$ is rather large, accounting for the strong undershooting of the histogram method from the asymptitic curve. Since we do not know the exact value of $C_2(\alpha_{q=1})$ in Eq. (17), it is not possible to obtain the deviation from the correct value, but the order of magnitude of the undershooting in Fig. 9 is consistent with the magnitude of $[\log(1/l)]^{-2}$.

V. THERMODYNAMIC INTERPRETATION

The method discussed in Sec. II can be understood as a canonical method of computing an entropy $f(\alpha)$.[13,23,37] To understand this statement, consider the thermodynamic formalism of multifractals.[12,13,16,23,37,38] The partition function $Z(\beta)$ for equal box sizes can be written as

$$Z(\beta)=\sum_i P_i^q(l)\sim l^{-\tau} . \tag{19}$$

Define a variable

$$E_i=-\ln(P_i) . \tag{20}$$

Then

$$Z(\beta)\equiv\sum_i \exp(-\beta E_i)=\sum_i \exp[q\ln(P_i)] . \tag{21}$$

Thus one can identify q with a Boltzmann temperature ($\beta=1/kT$), and E_i as the energy of the ith piece. Similarly, since the partition function can be rewritten as an exponential times a free energy (by convention[37] we absorb the temperature dependence in the free-energy function itself), using Eq. (19),

$$Z(\beta)\equiv\exp[-nF(\beta)]=\exp[-\tau\ln(l)] . \tag{22}$$

This identifies τ with the free energy. Similarly, one uses the Legendre transforms of the free energy to identify $f(\alpha)$ as an entropy and arrives at the following identifications:

$$q=\beta \quad \text{(inverse temperature)} , \tag{23}$$

$$\tau=F(\beta) \quad \text{(free energy)} , \tag{24}$$

$$f=S \quad \text{(entropy)} , \tag{25}$$

$$\alpha=U \quad \text{(internal energy)} . \tag{26}$$

The computations of the $f(\alpha)$ curve can be understood as the computation of the entropy versus internal energy curve of a statistical-mechanical system. To compute thermodynamic quantities (defined in the limit of $N\to\infty$) from finite samples, one usually considers a canonical ensemble, i.e., one weights different configurations with their Boltzmann weights and computes expectation values. This is precisely what Eqs. (6) and (7) do. The weighting term in those equations, which is given by Eq. (5) is [using Eqs. (20) and (23)]

$$\mu_i(q,l)=\frac{[P_i(l)]^q}{\sum_i[P_j(l)]^q}=\frac{\exp[-\beta E_i(l)]}{\sum_j \exp[-\beta E_j(l)]} . \tag{27}$$

This is precisely a Boltzmann weighting factor. Previous methods of direct determination of $f(\alpha)$ have attempted to use Eqs. (1) and (2) without incorporating all the corrections, and are simply computing thermodynamic averages via microcanonical ensembles. This assumes that the most probable value is also the average value [the statistical-mechanical interpretation of assuming that of a single dominant term approximation in evaluating the integral in Eq. (12) via steepest descent] and is correct only in the limit of $N \to \infty$. The severe finite-size effects in the form of logarithmic prefactors giving rise to overshoots or undershoots in the $f(\alpha)$ curve arise precisely due to this assumption and can be taken care of by using the canonical method. One should note that in turbulence, the range of scaling is decided by the Reynolds number, and these finite-size effects are large and cannot be neglected if one is studying a flow at low or moderate Reynolds numbers.

Two further comments: Firstly, if one first computes $\tau(q)$ and then Legendre transforms, then one can show that one gets a canonical average of the entropy.[26] This explains why such a procedure does not suffer from the undershoot or overshoot problems. It, however, suffers from the problems discussed in Sec. I. Secondly, the averaged value of α very often has direct physical interpretation; for an example, see Ref. 39.

VI. CONCLUSIONS

We have elaborated on a new method of determining $f(\alpha)$ directly from multifractal measures based on a canonical method of computing thermodynamic averages. We have shown that it is an accurate and simple method for the direct determination of $f(\alpha)$ from experimental data and eliminates the need to perform Legendre transforms of the D_q curves with the associated approximations involved in that procedure. We have also reviewed other methods recently proposed to measure $f(\alpha)$ directly from scale-invariant histograms. We have shown that the presence of logarithmic prefactors complicates the implementation of such methods considerably, and their neglect results in finite-size effects. Such methods may, however, be a useful alternative for cases where the determination of histograms at different scales can provide insight into the underlying statistical and self-similarity properties of the measure. If one is interested in the asymptotic $f(\alpha)$ curve, the canonical method is the best choice because of its simplicity and the absence of logarithmic corrections. This is particularly so when the $f(\alpha)$ curve possesses discontinuities corresponding to phase transitions.

ACKNOWLEDGMENTS

We are grateful to Peter W. Jones and Benoit Mandelbrot for many stimulating discussions. This work was supported by grants from the National Science Foundation.

APPENDIX A: LABORATORY EXPERIMENTS IN THE BOUNDARY LAYER

We consider measurements in air in a constant pressure turbulent boundary layer on a flat plate at a moderate Reynolds number. The free stream velocity of the flow is 12 m/s, the boundary-layer thickness δ is 4 cm at the measuring station, and the hot wire is located at a height above the wall of $y/\delta=0.2$. The hot wire is operated at an overheat ratio of 1.7 and the signal is low-pass filtered (roll-off rate at 18 dB per octave) with a DANTEC 55D26 signal conditioner at the noise floor (12.5 kHz) observed in the on-line power spectra (taken with an HP 3561 A spectrum analyzer). The signal is digitized with a 12-bit resolution on a MASSCOMP 5500 computer at a sampling rate of 25 kHz. Ten consecutive data files, each consisting of 10^6 points, are used for the analysis. The Kolmogorov microscale η is calculated from the signal according to

$$\eta=\left[\frac{\nu^2 U_c^2}{15\langle(\partial u_1/\partial t)^2\rangle}\right]^{1/4}, \tag{A1}$$

where U_c is the mean speed at the measuring station ($9m/s$), ν is the kinematic viscosity of air, and $\langle(\partial u_1/\partial t)^2\rangle$ is the measured average of the square velocity derivative. The result is $\eta=0.016$ cm. The Taylor microscale λ is calculated from the equation

$$\lambda=\frac{u_1' U_c}{\langle(\partial u_1/\partial t)^2\rangle^{1/2}}, \tag{A2}$$

where u_1' is the root mean square of the velocity fluctuations. This leads to a value of $\lambda=0.3$ cm. The Reynolds number R_λ based on the Taylor microscale is

$$R_\lambda=\frac{u_1'\lambda}{\nu}=110, \tag{A3}$$

which is moderate. The relatively short scaling range available for this flow will be specially suited as an illustrative test case for the various methods of computing $f(\alpha)$.

The rate of turbulent dissipation ε [defined in Eq. (8)] depends on the spatial gradients of the three velocity components' three coordinate directions. Now we assume that the square of the velocity gradient of one velocity component in only one direction is representative of the actual dissipation consisting of nine terms. These assumptions have been shown to be satisfactory in a slightly different context in Ref. 6. Also, as has been the practice, Taylor's hypothesis is used. This means that the time series of u_1 that is measured is considered as a linear cut through the frozen turbulent velocity field in the streamwise direction x_1. By measuring the $f(\alpha)$ curve with and without invoking the Taylor hypothesis, it was shown in Ref. 40 that this is a reasonable procedure in the context of passive scalar intermittency. Finally,

$$\varepsilon\sim\nu(1/U_c^2)\left[\frac{\partial u_2}{\partial t}\right]^2 \tag{A4}$$

where the derivative is obtained simply by finite differences. The total dissipation E_l occurring in a box of size l is normalized according to

$$E_l=\frac{\int_l \varepsilon\, dx}{\int \varepsilon\, dx}, \tag{A5}$$

where the integral in the numerator is performed within a segment of size l, and that in the denominator is over the entire data set of 10^7 points (approximately 4.10^4 integral length scales).

A problem arises due to the entrainment of fluid from outside the boundary layer when it occasionally reaches the hot wire in an irrotational state. One then observes extremely low values of dissipation, which produces very long tails on the left-hand side of the histograms of E_l.[20] This phenomenon has been observed before in two-dimensional slices of a turbulent jet[6] and in the wake of a circular cylinder. The choice to study the boundary layer was motivated, in part, because it was suspected that such "laminar" regions occurred much less frequently near the wall in that flow than on the center line of a "free shear flow" like the wake.

This "outer intermittency" is a dynamically different process, and (in any case) occurs quite rarely at the measurement station. Therefore it was attempted to eliminate such laminar regions from the data by setting an appropriate threshold and hold time on the dissipation. (The threshold and hold time were set entirely for purposes of identifying and eliminating the laminar regions, and were not changed during data processing.) This elimination could bias the results on the low-intensity regions of the distribution [right-hand side of the $f(\alpha)$ curve], but it was verified that there was no effect on the rest of the curve as a result of this procedure. The threshold that is used is a factor of 0.0054 times the mean dissipation within the turbulent region. The hold time used is $\Delta l = 10\eta$ (where Taylor's hypothesis has been used). Therefore if the total dissipation in a box size of Δl is less than $0.0054\ \langle \varepsilon \rangle \Delta l$, we simply eliminate from the data set not only that box but a large segment of size 200η centered around the original box. This eliminates a large fraction of the laminar regions without eliminating the very sparse, low-intensity dissipation regions that occur in the turbulent region. However, since some of the laminar regions will still be present (i.e., those just above the threshold), we expect the resulting histograms to be biased on their low-intensity tails, meaning that the $f(\alpha)$ will not be reliable on its rightmost part. A brief discussion of the effects of including the laminar regions has been given in Ref. 41.

APPENDIX B: EXPERIMENTS IN THE ATMOSPHERIC SURFACE LAYER

The data sets analyzed are the same as those used in Ref. 33. We consider measurements of the air speed on a windy day, at a height h of 2 m above the roof of a four story building. The mean velocity at the hot-wire location during the data acquisition is about 6 m/s. The hot wire is operated at an overheat ratio of 1.7 and the signal is low-pass filtered (roll-off rate of 18 dB per octave) with a DANTEC 55D26 signal conditioner at the observed noise floor of 3 kHz. Five data files, each 9×10^4 points long, were taken. The root mean square of the fluctuating velocity is about 42 cm/s $\pm 30\%$ and the Kolmogorov microscale computed according to (A1) is $\eta = 0.7$ cm. The Taylor microscale is about 2.5 cm. The Reynolds number $R_\lambda \sim 1500$. Again, ε is estimated using (A5) and E_l using (A6). For this flow we expect the inertial range to be quite large. Since the conditions of the experiment are quite uncontrollable, and the data sets are not intrinsically large as in the laboratory flows, we do not expect completely converged statistics. However, as shown in Ref. 33, the variations between different data sets are not too large ($\sim 10\%$ variability in $\alpha_{\min}$ and $\alpha_{\max}$). Here we use all five data sets together and perform the relevant sums over all 4.5×10^5 points.

*Present address: Center for Turbulence Research, Stanford University, Stanford, CA 94305-3030.

[1]B. B. Mandelbrot, J. Fluid Mech. **62**, 331 (1974).
[2]H. G. E. Hentschel and I. Procaccia, Physica **8D**, 435 (1983).
[3]U. Frisch and G. Parisi, in *Turbulence and Predictability of Geophysical Flows and Climate Dynamics,* edited by M. Ghil, R. Benzi, and G. Parisi (North-Holland, New York, 1985), p. 84.
[4]T. C. Halsey, M. H. Jensen, L. P. Kadanoff, I. Procaccia, and B. I. Shraiman, Phys. Rev. A **33**, 1141 (1986).
[5]C. Meneveau and K. R. Sreenivasan, Phys. Rev. Lett. **59**, 1424 (1987).
[6]R. R. Prasad, C. Meneveau, and K. R. Sreenivasan, Phys. Rev. Lett. **61**, 74 (1988).
[7]K. R. Sreenivasan and C. Meneveau, Phys. Rev. A **38**, 6287 (1988).
[8]L. de Arcangelis, S. Redner, and A. Coniglio, Phys. Rev. B **34**, 4656 (1986).
[9]P. Meakin, A. Coniglio, H. E. Stanley, and T. Witten, Phys. Rev. A **34**, 3325 (1986).
[10]H. J. Herrmann, Phys. Rep. **136**, 154 (1986).
[11]G. Paladin and A. Vulpiani, Phys. Rep. **156**, 147 (1987).
[12]B. B. Mandelbrot, in *Fluctuations and Pattern Formation, Cargèse,* edited by H. E. Stanley and N. Ostrowsky (Kluwer, Dordrecht, 1988).
[13]M. J. Feigenbaum, J. Stat. Phys. **46**, 919 (1987).
[14]M. J. Feigenbaum, J. Stat. Phys. **46**, 925 (1987).
[15]D. Ruelle, *Thermodynamic Formalism, Encyclopedia of Mathematics and its Applications* (Addison-Wesley, Reading, MA, 1978), Vol. 5.
[16]E. B. Vul, Y. G. Sinai, and K. M. Khanin, Russ. Math. Surv. **39**, 1 (1984).
[17]Tamas Tel, Z. Naturforsch. **43a**, 1154 (1988).
[18]E. Ott, W. D. Withers, and J. A. Yorke, J. Stat. Phys. **36**, 687 (1984).
[19]P. Grassberger, R. Badii, and A. Politi, J. Stat. Phys. **51**, 135 (1988).
[20]C. Meneveau and K. R. Sreenivasan, Phys. Rev. A **137**, 103 (1989).
[21]R. Badii and G. Broggi, Phys. Lett. **131A**, 131 (1988).
[22]W. van de Water and P. Schram, Phys. Lett. A **37**, 3188 (1988).
[23]A. Chhabra and R. V. Jensen, Phys. Rev. Lett. **62**, 1327 (1989).

[24]H. G. Eggleston, Q. J. Math. Oxford Ser. **20**, 31 (1949).
[25]P. Billingsley, *Ergodic Theory and Information* (Wiley, New York, 1965).
[26]M. H. Jensen, L. P. Kadanoff, and I. Procaccia, Phys. Rev. A **36**, 1409 (1987).
[27]A. N. Kolmogorov, C. R. Acad. Sci. U.S.S.R. **30**, 301 (1941); **30**, 538 (1941).
[28]A. N. Kolmogorov, J. Fluid Mech. **13**, 82 (1962).
[29]A. M. Oboukhov, J. Fluid Mech. **13**, 77 (1962).
[30]B. B. Mandelbrot, *Turbulence and Navier-Stokes Equations,* edited by R. Teman (Springer, Berlin, 1976).
[31]R. Benzi, G. Paladin, G. Parisi, and A. Vulpiani, J. Phys. A **17**, 3521 (1984).
[32]K. R. Sreenivasan and C. Meneveau, J. Fluid Mech. **173**, 357 (1986).
[33]C. Meneveau and K. R. Sreenivasan, Nucl. Phys. B (Proc. Suppl.) **2**, 49 (1987).
[34]U. Frisch, P. L. Sulem, and M. Nelkin, J. Fluid Mech. **87**, 719 (1978).
[35]C. Meneveau, Ph.D. thesis, Yale University, 1989 (unpublished).
[36]A. Arneodo, G. Grasseau, and E. J. Kostlich, Phys. Lett. **124A**, 424 (1987).
[37]M. J. Feigenbaum, J. Stat. Phys. **25**, 669 (1978).
[38]J. L. McCauley (unpublished).
[39]Carl Evertsz and J. W. Lyklema, Phys. Rev. Lett. **58**, 397 (1985).
[40]K. R. Sreenivasan, R. R. Prasad, C. Meneveau, and R. Ramshankar, Pure Appl. Geophys. **131**, 297 (1989).
[41]R. R. Prasad and K. R. Sreenivasan, J. Fluid Mech. (to be published).